Hydration and Proton Conduction in Nafion/Ceramic Nanocomposite Membranes Produced by Solid-State Processing of Powders from Mechanical Attrition

Amanda L. Moster, Brian S. Mitchell

Department of Chemical and Biomolecular Engineering, Tulane University, New Orleans, LA 70118

Received 3 November 2008; accepted 21 January 2009
DOI 10.1002/app.30131
Published online 16 March 2009 in Wiley InterScience (www.interscience.wiley.com).

ABSTRACT: A solid-state method of Nafion/ceramic nanocomposite membrane preparation was used. Nanocomposite powders from Nafion pellets and a zirconium phosphate ceramic were formed by mechanical attrition. The powders were consolidated into membrane form by mechanical pressing. A decrease in the particle size and improved dispersion of the ceramic within the polymer phase were confirmed with scanning electron microscopy. An evaluation of membrane hydration by thermogravimetric analysis indicated that the prepared membranes had increased water uptake in comparison with a commercially available membrane. However, as the distribution of the ceramic was improved, the hydration of the sample was reduced. Low-temperature differential scanning calorimetry indicated that the additional water contributed to an increase in the contents of both freezing and nonfreezing water in the membranes. Proton conductivity testing at various relative humidities and temperatures revealed that the prepared membranes had conductivities comparable to but somewhat lower than those of the commercial membranes. An increase in conductivity was seen with decreased particle size and improved dispersion of the ceramic. © 2009 Wiley Periodicals, Inc. J Appl Polym Sci 113: 243–250, 2009

Key words: fluoropolymers; membranes; nanocomposites

INTRODUCTION

Polymer electrolyte membrane fuel cells (PEMFCs) are promising alternatives to internal combustion engines in light-duty transportation applications because of their fast start-up capability and relatively low operating temperatures.[1] At the heart of PEMFCs is the proton-conducting membrane. This solid polymer electrolyte acts as a barrier to electron flow between the anode and cathode, while readily allowing the transport of protons to complete the electrical circuit of the fuel cell. The most common electrolyte used in PEMFCs is the perfluorinated sulfonic acid ionomer Nafion. Patented in 1966 by DuPont de Nemours,[2] Nafion remains the benchmark polymer electrolyte membrane against which other prospective electrolytes are compared today.[3]

Nafion's molecular architecture can be described as that of a copolymer (Fig. 1). The molecule's tetrafluoroethylene backbone has been found to organize into crystalline regions similar to those of polytetrafluoroethylene. These regions are hydrophobic in nature and provide the membrane's mechanical strength and chemical stability. In response to these hydrophobic regions, the perfluorinated pendent side chains, terminated by SO_3H functional groups, aggregate to form hydrophilic clusters.[4,5] These clusters, also called pores, swell and aggregate upon hydration of the ionomer. The structure and organization of the domains in hydrated membranes have been debated and modeled extensively.[4,6,7] Although each model suggests a different shape and distribution of the hydrophilic and hydrophobic domains, each includes aggregation of the ionic groups into clusters, which together form a network for polar solvent and ionic transport.

Conductivity in Nafion has been found to be dependent on the level of hydration in the membrane.[8,9] Thus, understanding how water molecules interact with the local environment within the ionic pores is important. One method that has been used for this purpose is low-temperature differential scanning calorimetry (DSC).[10,11] From such studies, water molecules have been found to have varying levels of interaction with the structure of the ionomer. The water within Nafion membranes can be classified as either freezable or nonfreezable. Nonfreezable water

Correspondence to: B. S. Mitchell (brian@tulane.edu).
Contract grant sponsor: Tulane Institute for Macromolecular Engineering and Science.
Contract grant sponsor: National Aeronautics and Space Administration; contract grant numbers: NCC3-946 and NNC06AA18A.

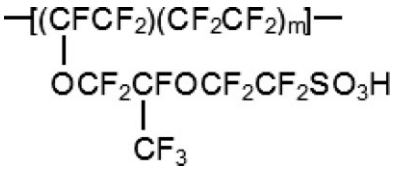

Figure 1 Structure of Nafion.

is composed of molecules that are strongly associated with either the polymer backbone or ionic groups. It is located in primary hydration shells within the pore structure. These water molecules show no thermal transitions. Freezable water can be found in secondary and higher hydration shells and has been found to exhibit a freezing exotherm similar to that of bulk water around −20°C.

In this work, Nafion and Nafion/ceramic composite membranes were manufactured by a solid-state processing technique termed near net-shape manufacturing (NNSM). As described previously,[12] NNSM is a two-step process involving the formation of powders via mechanical attrition (milling, comilling, or cryomilling) followed by consolidation with pressing (cold, hot, or isostatic pressing). The NNSM technique has been shown to be an effective method for producing Nafion-based nanocomposite membranes via a completely solid-state route. The overall membrane water content and the fractions of freezable water versus nonfreezable water were quantified and compared to those of commercially available membranes. Proton conductivity measurements were also carried out on the membranes so that the relationship between membrane hydration and proton conduction in the NNSM membranes could be explored.

EXPERIMENTAL

Nafion membranes were manufactured with materials and methods previously described.[12] Briefly, Nafion pellets with an equivalent weight of 1100 were first ion-exchanged with tetrabutylammonium hydroxide to create a melt-processable form of the ionomer.[13] Powders were then created from the Nafion TBA+ pellets by mechanical attrition at a cryogenic temperature. The resulting powders were mechanically pressed into membrane form at 190°C with a heated platen press and then converted back to the acid form of the ionomer for further testing. None of the membranes discussed in this work were processed by hot isostatic pressing, as was done in the previous study.

Composite membranes were created via the comilling of Nafion TBA+ pellets with PRONAS (Ceramatec, Inc., Salt Lake City, UT), a zirconium phosphate proton-conducting ceramic. PRONAS was supplied by the manufacturer in powdered form. It was used "as is" or was subjected to further particle size reduction via high-energy ball milling (HEBM). HEBM was conducted with a Spex 8000D mixer mill (Spex CertiPrep, Metuchen, NJ). The milling medium was the Spex 8005 zirconia mixing vial set, which consisted of a grinding vial and two 1.27-cm (0.5-in.) milling balls. A 2 : 1 ball-to-powder mass ratio was used, and samples were milled for a total of 3 h. Samples containing 5 wt % ceramic were created, as noted in Table I. Membranes were formed by the consolidation of the resulting powders in a platen press as described previously.

A commercial Nafion membrane with a 10-mil thickness and an equivalent weight of 1110 (N1110, Ion Power, Inc., New Castle, DE) was obtained and tested along with the nanocomposite membranes. For consistency, the membrane was pretreated via boiling in 4*M* methanolic H_2SO_4, as described in our previous study.[12]

Scanning electron microscopy (SEM) was used previously to determine the particle size of the milled Nafion and composite powders.[12] Further analysis was conducted in this work to determine the effect of HEBM on the particle size of PRONAS. Imaging was conducted for the PRONAS ceramic powder both before and after HEBM. Powder samples were dispersed in excess methanol by sonication. A small drop of the suspension was placed onto a clean glass coverslip, and the solvent was allowed to evaporate. The coated coverslip was then adhered to the SEM stub with carbon tape and gold-coated for viewing at an accelerating voltage of 3 kV. SEM was also used for a cross-sectional analysis of the NNSM5H membrane to determine the distribution of the ceramic within the polymer phase. The experimental methods used were the same as those previously reported.[12]

TABLE I
Compositions and Formation Methods of the Membranes

Sample	Description	PRONAS content (wt %)	HEBM time (min)	Cryogenic milling time (min)
NNSM	Near-net-shape-manufactured Nafion membrane (cryomilling)	0	0	6
NNSM5	Near-net-shape-manufactured composite membrane (cryomilling)	5	0	6
NNSM5H	Near-net-shape-manufactured composite membrane (HEBM and cryomilling)	5	180	30
N1110	Commercial Nafion membrane (10-mil thickness)	—	—	—

Wide-angle X-ray diffraction (WAXD) was performed on PRONAS powders to determine the effect of HEBM on the crystallite size and on NNSM and commercial membranes to evaluate the effects of the processing technique and the addition of ceramic on the ionomer's structure. Tests were conducted on a Scintag XDS 2000 (Waltham, MA) with a Cu Kα radiation source operating at 43 kV and 38 mA. Samples were tested at room temperature and humidity at a scan rate of 1°/min over a 2θ scan range of 5–60°.

The water uptake of the fully hydrated membranes was determined by thermogravimetric analysis (TGA; TGA 2950, TA Instruments, New Castle, DE), as formerly described.[12] The gravimetric data were further used to calculate the total number of water molecules per cation-exchange site (λ):

$$\lambda = \frac{M_{wet} - M_{dry}}{18 M_{dry}} \times EW \quad (1)$$

where M_{wet} and M_{dry} are the masses of the membrane sample in its fully hydrated and dehydrated states, respectively, and EW represents the equivalent weight of the ionomer.

DSC was used to evaluate the freezing and nonfreezing water contents of the membranes. Tests were conducted on a DSC 2950 (TA Instruments) with a liquid-nitrogen cooling accessory. Membranes were prepared by boiling in deionized water for 60 min to achieve complete hydration. Samples weighing 5–10 mg were cut from the hydrated membranes and stored in water at room temperature until use. At test time, a sample was removed from the water and blotted dry of surface moisture with a sterile tissue. It was then immediately placed into an aluminum, nonhermetic sample pan and covered with a lid to prevent water loss. The pan was left unsealed. The sample was transferred to the test chamber, and data collection was promptly started. Measurements were carried out from room temperature to −50°C at a cooling rate of 1°C/min. The temperature was then increased to 50°C at the same rate. An empty aluminum sample pan and lid were used as the reference. Data analysis was conducted with Universal Analysis software (TA Instruments).

The quantities of freezable water (N_{fre}) and nonfreezable water (N_{non}) in an ionomer membrane, expressed as molecules of water per sulfonic acid group, were determined with eqs. (2) and (3).[10] N_{fre} is equivalent to the ratio of the mass of freezable water (M_{fre}) to the total mass of water (M_{tot}) in the membrane. M_{wet}, M_{dry}, and λ are the TGA results discussed previously. The enthalpy of freezing (H_{fre}) is found by the integration of the exothermic peak associated with the freezing of water within the membrane. H_{ice} is the literature value of the melting enthalpy of ice:

$$N_{fre} = \frac{M_{fre}}{M_{tot}} \times \lambda = \frac{H_{fre}/H_{ice}}{(M_{wet} - M_{dry})/M_{wet}} \times \lambda \quad (2)$$

$$N_{non} = \lambda - N_{fre} \quad (3)$$

The proton conductivity of the membranes was determined with the four-probe method[14] in both liquid water and relative humidity (RH) environments. Measurements taken in liquid water were conducted at 60°C as described previously.[12] Testing conducted in RH environments was performed by BekkTech, LLC (Loveland, CO). Tests were conducted at 60, 80, and 120°C. Samples were stored at room temperature and humidity before testing. Each sample was loaded into the test cell and allowed to equilibrate at 60°C and 70% RH for 2 h. The RH within the cell was then systematically reduced to 20% before being increased to 100%. Adequate time was allotted (15–60 min) for the system to reach equilibrium at each temperature and RH. During testing, the cell pressure was maintained at 100 kPa, and a flow rate of 1000 SCCM of hydrogen carrier gas was used. The temperature in the cell was next increased to 80°C, and the procedure of wet-up at 70% RH for 2 h followed by data collection (again at 100 kPa and 1000 SCCM hydrogen) was repeated. Next, the test was conducted for a third time at 120°C. This time, the cell pressure was maintained at 230 kPa with a hydrogen flow rate of 500 SCCM. Membrane conductivity was calculated as follows:

$$\sigma = \frac{L}{RWT} \quad (4)$$

where σ represents the proton conductivity (S/cm); R is the sample resistance (Ω); and L, W, and T are the sample length (cm), width (cm), and thickness (cm), respectively. Sample dimensions used for the calculations were taken before the sample wet-up.

RESULTS AND DISCUSSION

SEM photomicrographs of PRONAS ceramic before and after HEBM appear in Figure 2. PRONAS ceramic powder, as supplied by the manufacturer, consisted of agglomerated particles with dimensions that ranged from approximately 100 nm to more than 1 μm. After the HEBM procedure, the particle size was more consistent and ranged from approximately 50 to 500 nm. An examination of the membrane cross section revealed that the ceramic agglomerates present in the NNSM5H membrane were generally smaller in size and more evenly distributed within the membrane in comparison with the NNSM5 membrane discussed previously (Fig. 3).[12] This improved dispersion of the ceramic phase within the membrane was most likely the result of

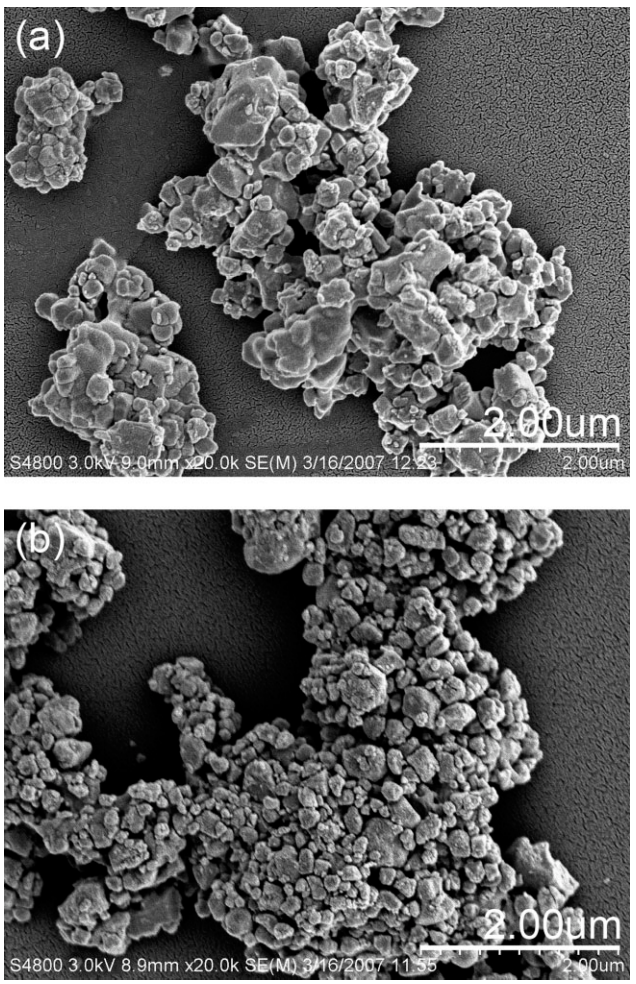

Figure 2 SEM photomicrographs of PRONAS ceramic: (a) as supplied by the manufacturer and (b) following HEBM.

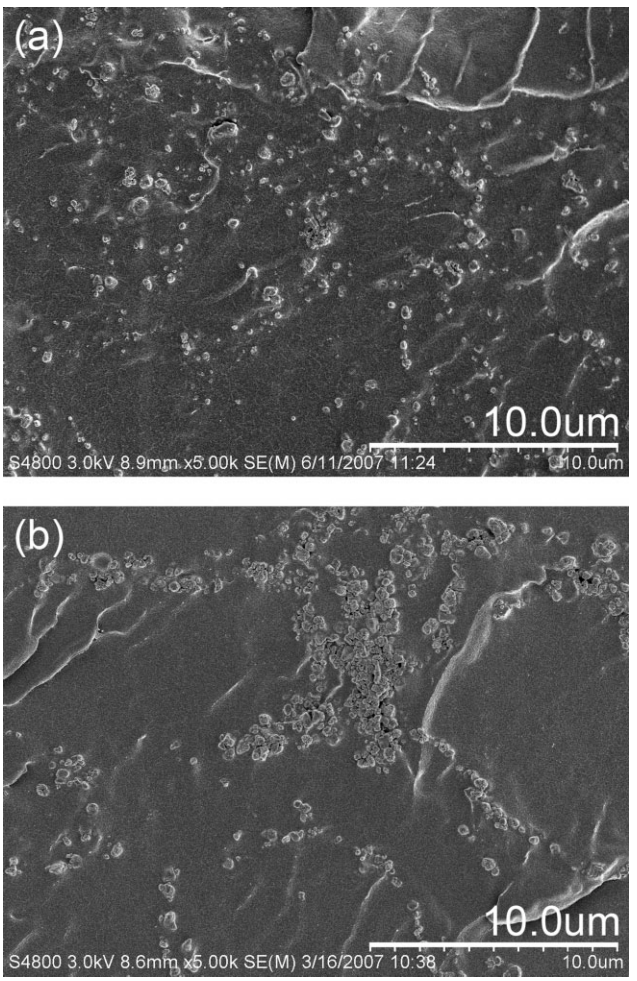

Figure 3 SEM photomicrographs of membrane cross sections of (a) NNSM5H and (b) NNSM5.

the additional cryogenic milling time used during the formation of the nanoparticles. The increase in the milling time from 6 min (used for the preparation of NNSM and NNSM5 samples) to 30 min allowed for more intimate mixing of the polymer and ceramic components, which in turn reduced ceramic particle agglomeration.

WAXD was performed on PRONAS ceramic both before and after HEBM to assess the effect of the procedure on the ceramic's crystallite size. An analysis of the results with the method of Scherrer and Wilson[15] revealed a decrease in the crystallite size from an average value of 114 nm in the "as is" PRONAS sample to 100 nm following mechanical attrition.

WAXD was also conducted on the membrane samples to determine the effect of the processing technique on the ionomer morphology. Diffraction profiles are compared in Figure 4. All membranes were found to have two characteristic reflections. The reflection centered at $2\theta = 39^\circ$ has been attributed to the crystallinity within the perfluorocarbon chains of the ionomer.[16] A comparison of this reflection for the N1110 and NNSM membranes showed no differences in peak height or shape, although measurement of the full width at half-maximum (FWHM) indicated that the NNSM peak was

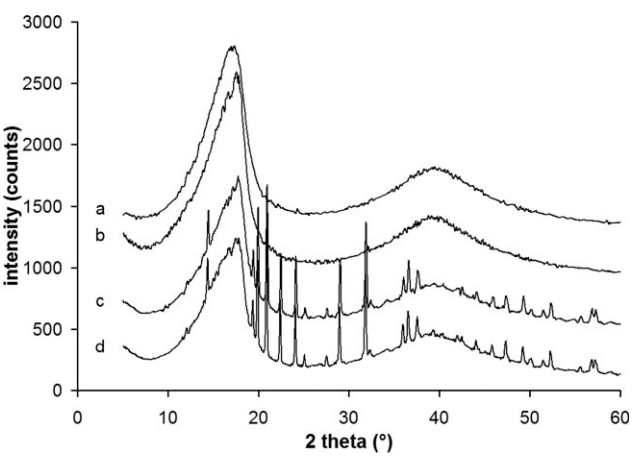

Figure 4 WAXD profiles of Nafion and composite membranes: (a) N1110, (b) NNSM, (c) NNSM5, and (d) NNSM5H.

narrower with an FWHM of 9.24° versus the N1110 FWHM of 9.49°, suggesting higher crystallinity in the NNSM sample. The second reflection at $2\theta = 17.5°$ could be deconvoluted into two peaks associated with the crystalline ($2\theta = 17.5°$) and amorphous ($2\theta = 16°$) components of the perfluorocarbon chains. The ratio of the two peak areas could provide the crystallinity percentage of the polymer.[17,18] A comparison of these peaks for the NNSM and N1110 membranes found an obvious leaning of the NNSM reflection toward a higher diffraction angle. Measurement of FWHM of the reflections showed that the NNSM membrane had a slightly smaller FWHM of 4.60° versus 4.69° measured for the N1110 sample. Both the leaning of this peak and narrowing of both characteristic reflections suggested a higher level of crystallinity in the NNSM sample.[19,20] This increase in crystallinity was likely due to the high temperature (190°C) used during the hot-pressing step of the membrane formation procedure.[21]

The addition of ceramic to the membrane in the NNSM5 and NNSM5H samples gave the usual reflection at $2\theta = 39°$ for Nafion with additional reflections associated with the ceramic phase. As was found for the NNSM membrane, the reflections at $2\theta = 17.5°$ leaned toward the higher diffraction angle. FWHM was 4.40° for the NNSM5 sample, suggesting increased crystallinity versus that of the pure Nafion membranes. An increase in crystallinity due to the incorporation of an inorganic component is common.[17–19] FWHM of the NNSM5H sample was 4.68°, similar to that of the commercial membrane. The additional mechanical attrition used during the formation of this composite resulted in increased dispersion of the ceramic within the ionomer, which may have inhibited crystal phase growth.

TGA and DSC were used together to evaluate the hydration properties of the membranes. From the TGA results, the water uptake percentage and number of water molecules per sulfonic acid group (λ) were calculated (Table II). As discussed in our previous work,[12] membranes created by NNSM were able to achieve a significantly higher level of maximum hydration than the extruded commercial product. The NNSM membrane was found to absorb 71.7 wt % as opposed to 48.7 wt % in the commercial sample tested here. The addition of 5 wt % ceramic in its "as is" state had little effect on the membrane water uptake. However, the sample containing high-energy-ball-milled ceramic had a somewhat reduced water uptake of just 62.6 wt %.

Low-temperature DSC was used to examine the types of water within the membranes. Sample DSC plots obtained for the NNSM and N1110 samples appear in Figure 5. The exothermic peak seen around −20°C is associated with the freezing of water within the membrane. It appeared at a subzero temperature because of the effect of supercooling.[22] During the freezing transition, the temperature of the NNSM sample increased by approximately 1°C. Additionally, a loop can be seen in the DSC trace. During crystallization of the water, latent heat was released so rapidly that it was incorporated into the heat capacity of the sample rather than being released directly to the environment. This resulted in a temperature increase of the sample, as noted in the plots. An endotherm associated with the melting of water can be seen around −2°C for the various samples. Although not shown here, the DSC plots associated with the composite membrane samples have features similar to those of the NNSM membrane.

As discussed previously, the water molecules within a Nafion membrane have varying levels of interaction with the ionomer's structure.[10,11,23] Molecules located near the pore wall within the hydrophilic domains interact strongly with the ionic groups, so strongly in fact that they are unable to freeze and show no characteristic thermal transition in DSC. The water that exists more internally within the pore structure lacks the intimate ionic interaction and is able to behave more like bulk water and undergo a freezing transition. The water associated with the DSC peaks presented here is that of the secondary and higher hydration shells and is referred to as the freezing water.

Equations (2) and (3) were used to quantify the amounts of freezing water versus nonfreezing water in the membranes.[10] TGA provided the wet and dry membrane masses and allowed for the calculation of λ, as described previously. H_{fre} was found by the

TABLE II
Results of TGA and DSC Analysis

Sample	Average peak temperature (°C)	Average H_{fre} (J/g)	H_2O uptake (%)	λ (H_2O/SO_3H)	N_{fre} (H_2O/SO_3H)	N_{non} (H_2O/SO_3H)	N_{fre}/N_{non}	N_{fre}/λ
N117[a]	—	30.2	—	20.8	7.7–8.3	12.5–13.1	0.63	0.39
N1110	−21.2	47.5	48.7	29.8	12.9–13.9	15.9–16.9	0.82	0.45
NNSM	−15.9	73.1	71.7	43.8	23.0–24.7	19.2–20.9	1.19	0.54
NNSM5	−17.6	71.6	70.7	43.2	22.4–24.0	19.2–20.8	1.16	0.54
NNSM5H	−19.6	67.5	62.6	38.2	20.1–21.6	16.7–18.1	1.20	0.55

[a] Data from Saito et al.[10]

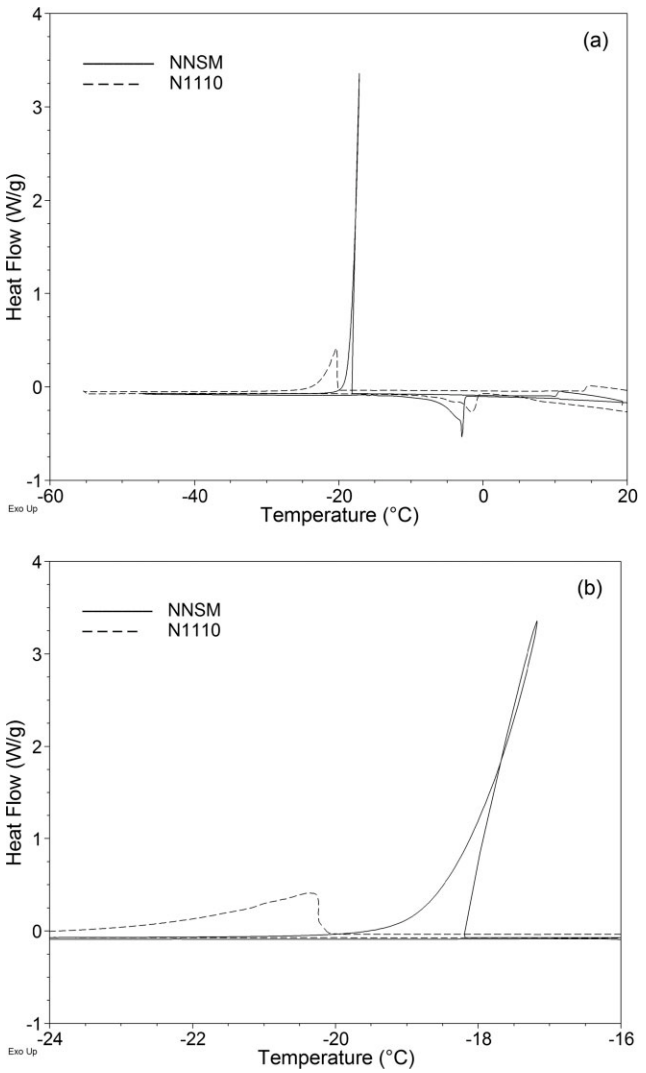

Figure 5 DSC thermograms of NNSM and N1110 membranes: (a) complete test results showing freezing and melting transitions of water within the membranes and (b) zoomed-in view of the freezing exotherms.

integration of the exothermic peak found by DSC. A range of literature values (311–334 J/g) was used for H_{ice}.[24] Results of the analysis appear in tabulated form in Table II, and freezing water and nonfreezing water are compared graphically in Figure 6. Also shown in Table II and Figure 6 are the results found by Saito et al.[10] for the same testing conducted on the commercially available Nafion membrane N117 (equivalent weight of 1100 and 7-mil thickness).

As stated previously, the near-net-shape-manufactured membranes had increased water uptake in comparison with the commercial N1110 membrane. From the DSC analysis, more can be learned about the interaction of this additional water with the polymer structure. Results for the N117 membrane tested by Saito et al.[10] are included in Table II for comparison. The difference in water uptake of the N1110 and N117 commercial membranes was likely due to differences in the pretreatment conditions, as discussed previously.[12] The fully hydrated N1110 membranes were found to have a λ value of 29.8 H_2O/SO_3H, 45% of which existed as freezable water. In the NNSM membranes, λ was found to be 43.8 H_2O/SO_3H. N_{fre} and N_{non} were increased in comparison with those of the commercial membrane. However, a greater portion of molecules fell into the freezable category, resulting in an increase in the percentage of freezable water (N_{fre}/λ) to 54%. The addition of 5 wt % ceramic (NNSM5) to the membrane had a minimal effect on the water uptake and distribution between freezable and nonfreezable states in comparison with the pure Nafion NNSM membrane. When the ceramic had been high-energy-ball-milled (NNSM5H), the overall water uptake decreased to 38.2 H_2O/SO_3H. The percentage of freezable water remained about the same at 55%, so both N_{fre} and N_{non} decreased. This was likely the result of the improved distribution of the ceramic within the ionomer phase discussed previously. The decreased N_{non} value suggests increased interaction between the ceramic and ionic groups of the polymer and therefore decreased interaction of water with the groups. Additionally, the incorporated ceramic limited N_{fre} by restricting the overall swelling of the membrane.

The ratio of freezable water to nonfreezable water in membranes is significant because the different types of water play different roles in proton conduction. The freezable water within a swollen ionomer membrane is responsible for the majority of proton conduction as it behaves as bulklike water and improves proton mobility. As the level of hydration of the membrane is reduced, so too is the quantity of freezable water.[11] The result is decreased proton conductivity.[8,9] Conductivity measurements conducted on fully hydrated membranes at temperatures low enough to crystallize the freezable water

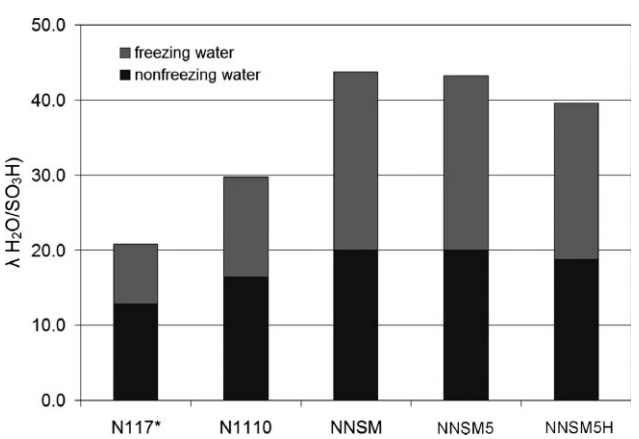

Figure 6 Quantitative comparison of freezing and nonfreezing water contents of the membrane samples (*data from Saito et al.[10]).

TABLE III
Results of the Proton Conductivity Testing

Conditions	Conductivity (mS/cm)				
	NNSM	NNSM5	NNSM5H	N117[b]	N112[b]
60°C					
20% RH	1.1	1.0	2.3	—	4.5
60% RH	18.3	18.4	20.8	—	25.9
100% RH	96.5	76.7	102.1	—	119.6
Liquid H_2O[a]	116.2	115.5	—	—	—
80°C					
20% RH	1.2	1.2	2.2	3.4	4.2
60% RH	22.7	20.6	27.6	31.1	34.4
100% RH	136.5	131.1	130.6	97.9	145.2
120°C					
20% RH	1.6	1.5	2.7	4.9	4.2
60% RH	27.5	26.7	34.7	47.8	47.9
100% RH	184.5	175.2	177.1	210.0	193.7

Select proton conductivity data were measured as the RH was increased.
[a] Data collected by Moster and Mitchell.[12]
[b] Data provided by BekkTech, LLC, for comparison.

have indicated that a low level of conductivity still exists. The nonfreezable water assists with the transport of protons in this situation.[11] Thus, both types of water are important to proton conduction. For fuel cell operation above freezing, the quantity of freezable water should be maximized within the membrane, whereas operation at temperatures below the freezing point of water will likely benefit from the presence of additional nonfreezing water within the membrane.[10,11]

The proton conductivity of fully hydrated NNSM, NNSM5, and N1110 membranes was determined in liquid water at 60°C previously.[12] The tabulated results appear in Table III. Conductivity analysis in RH environments was conducted by BekkTech on NNSM, NNSM5, and NNSM5H membranes. Data for commercial Nafion membranes N117 and N112 (7- or 2-mil thickness, respectively, and equivalent weight of 1100) were provided by BekkTech for comparison.

Overall, the conductivities of the near net-shape membranes were comparable to, but lower than, those of the commercial membrane. Differences were smallest at a high humidity and more pronounced as the RH approached 20%. The NNSM and NNSM5 membranes had very similar proton conductivities at all temperature and humidity levels tested. The addition of the PRONAS ceramic in its "as is" state had no apparent effect, as was found when these membranes were tested in water at 60°C (Table III). An improvement in conductivity was seen for the NNSM5H sample. The enhancement was most prominent at a low humidity, at which the conductivity increased by as much as twofold over that of the NNSM membrane. An analysis of the ceramic powders and membrane cross sections by SEM (discussed previously) found that the particle size of the ceramic was reduced by HEBM. Additionally, the extended comilling time in the cryogenic mill (Table I) resulted in improved dispersion of the ceramic phase within the Nafion matrix. The improvement in conductivity can be attributed to both of these factors.

Figure 7(a,b) presents the results of testing in RH environments at 60 and 120°C, respectively. Data for a commercial N112 membrane are included for comparison. As discussed in the Experimental section, data collection began at 70% RH at the test temperature. During the first phase of the test, the RH was incrementally decreased to 20%. Immediately afterward, the RH in the test cell was increased to 100% in the same manner. The RH in the test cell was controlled by the variation of the humidity of the carrier gas stream that flowed continuously through the cell. The temperature of the cell itself was held constant. As a result of this technique, the conductivity of the membranes was measured twice in the range of 30–70% RH, as can be seen on the plots.

An examination of the N112 plots reveals that the conductivity measured during the RH downsweep was greater than that measured as RH was

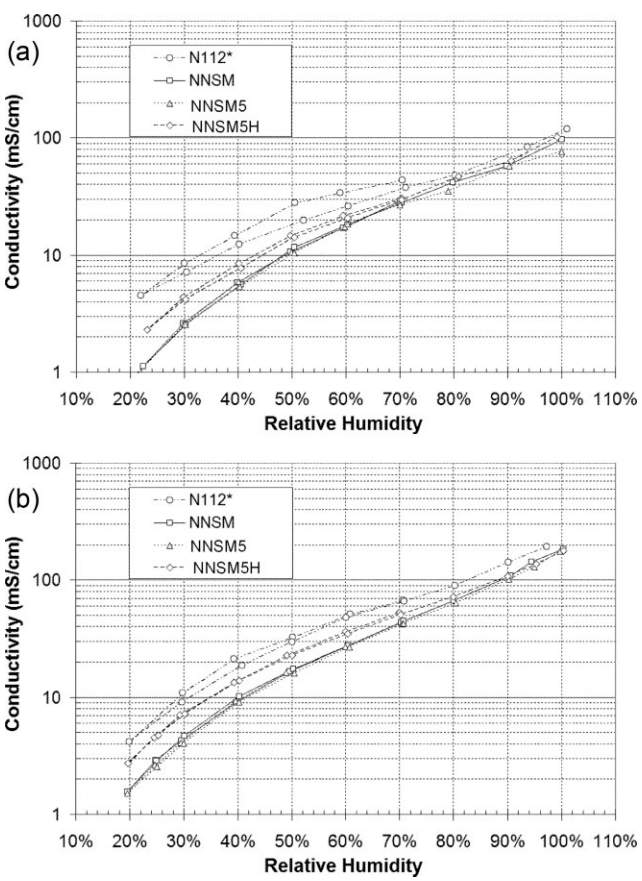

Figure 7 Membrane proton conductivity measured at various RHs and at (a) 60 or (b) 120°C (*data provided by BekkTech, LLC, for comparison).

increased. The effect was most pronounced at low temperatures. This hysteresis in the measured conductivity is due to different levels of membrane hydration. The degree of hydration achieved by a Nafion membrane is a function of the temperature and RH of the environment, with maximum hydration achieved by the boiling of the membrane in liquid water. Within the experimental parameters and allotted equilibration times of the experiments conducted here, the N112 membrane was not able to rehydrate to the same extent, and conductivity was compromised. Conversely, the membranes created by the near net-shape technique showed very little of this hysteresis. Their hydration was quickly restored to the previous level.

CONCLUSIONS

In a continuation of a previous study, reduced particle and crystallite size and improved distribution of the PRONAS proton-conducting ceramic within Nafion membranes was achieved with NNSM. Analyses by SEM and WAXD of ceramic powders and SEM of membrane cross sections proved both efforts to be successful.

Am evaluation of the membrane water uptake and distribution between freezing and nonfreezing states was accomplished via TGA and low-temperature DSC experiments. Near net-shape membranes were found to have increased water uptake. The uptake was greatest and nearly equivalent for the NNSM and NNSM5 membranes, which absorbed 43–44 H_2O/SO_3H. This corresponded to a 13–14 H_2O/SO_3H increase over the commercial N1110 membrane tested. Low-temperature DSC experiments confirmed that the quantities of both the freezing and nonfreezing water were increased. The additional milling used in the preparation of the NNSM5H sample resulted in a somewhat reduced overall water content of 38 H_2O/SO_3H. The reduced water uptake was attributed to the reduced particle size and improved distribution of the ceramic phase.

Proton conductivity testing at different temperatures and various RHs revealed that the near net-shape membranes were able to quickly equilibrate to the level of humidity in their environment and more so than the commercially available membranes. However, regardless of this quick equilibration and enhanced water uptake, their conductivity remained lower than that of the commercial samples. The differences were most significant at a low humidity and more minimal at a high humidity. Results for NNSM and NNSM5 membranes mirrored those found when membranes were previously tested at 60°C in water and indicated that the addition of the ceramic to these membranes had no apparent effect on the conductivity properties. The addition of the high-energy-ball-milled ceramic to the NNSM5H sample did result in improved conductivity, especially at a low humidity.

The authors are grateful to Ceramatec, Inc. (Salt Lake City, UT), for supplying the PRONAS ceramic and to Shekar Balagopal of Ceramatec for technical discussions.

References

1. Hydrogen Fuel Cells & Infrastructure Technology Program; Washington, D.C., 2007; DOE/GO-102007–2430.
2. Connolly, D. J.; Gresham, W. F. U.S. Pat.3,282,875 (1966).
3. Diat, O.; Gebel, G. Nat Mater 2008, 7, 13.
4. Mauritz, K. A.; Moore, R. B. Chem Rev 2004, 104, 4535.
5. Rollet, A.-L.; Diat, O.; Gebel, G. J Phys Chem B 2002, 106, 3033.
6. Paddison, S. J. Annu Rev Mater Res 2003, 33, 289.
7. Kreuer, K.-D.; Paddison, S. J.; Spohr, E.; Schuster, M. Chem Rev 2004, 104, 4637.
8. Zawodzinski, T. A., Jr.; Derouin, C.; Radzinski, S.; Sherman, R. J.; Smith, V. T.; Springer, T. E.; Gottesfeld, S. J Electrochem Soc 1993, 140, 1041.
9. Anantaraman, A. V.; Gardner, C. L. J Electroanal Chem 1996, 414, 115.
10. Saito, M.; Hayamizu, K.; Okada, T. J Phys Chem B 2005, 109, 3112.
11. Siu, A.; Schmeisser, J.; Holdcroft, S. J Phys Chem B 2006, 110, 6072.
12. Moster, A. L.; Mitchell, B. S. J Appl Polym Sci 2009, 111, 1144.
13. Moore, R. B.; Cable, K. M.; Croley, T. L. J Membr Sci 1992, 75, 7.
14. Lee, C. H.; Park, H. B.; Lee, Y. M.; Lee, R. D. Ind Eng Chem Res 2005, 44, 7617.
15. Klug, H. P.; Alexander, L. E. X-Ray Diffraction Procedures for Polycrystalline and Amorphous Materials, 2nd ed.; Wiley: New York, 1974; p 662.
16. Starkweather, H. W., Jr. Macromolecules 1982, 15, 320.
17. Antonucci, P. L.; Arico, A. S.; Creti, P.; Ramunni, E.; Antonucci, V. Solid State Ionics 1999, 125, 431.
18. Dimitrova, P.; Friedrich, K. A.; Stimming, U.; Vogt, B. Solid State Ionics 2002, 150, 115.
19. Jiang, R.; Kunz, H. R.; Fenton, J. M. J Membr Sci 2006, 272, 116.
20. Moore, R. B., III; Martin, C. R. Macromolecules 1988, 21, 1334.
21. Gebel, G.; Aldebert, P.; Pineri, M. Macromolecules 1987, 20, 1425.
22. Mishima, O.; Stanley, H. E. Nature 1998, 396, 329.
23. Kim, Y. S.; Dong, L.; Hickner, M. A.; Glass, T. E.; Webb, V.; McGrath, J. E. Macromolecules 2003, 36, 6281.
24. Petrenko, V. F.; Whitworth, R. W. Physics of Ice; Oxford University Press: New York, 1999.